Atomic collisions with relativistic heavy ions. VIII. Charge-state studies of relativistic uranium ions

R. Anholt, W. E. Meyerhof, and X.-Y. Xu*
Department of Physics, Stanford University, Stanford, California 94305

Harvey Gould
Materials and Molecular Research Division, Lawrence Berkeley Laboratory, University of California, Building 71-259, Berkeley, California 94720

B. Feinberg and R. J. McDonald
Accelerator and Fusion Division, University of California, Lawrence Berkeley Laboratory, Berkeley, California 94720

H. E. Wegner and P. Thieberger
Department of Physics, Brookhaven National Laboratory, Upton, New York 11973
(Received 26 February 1987)

Charge-state distributions were measured for incident 105-, 220-, 430-, and 955-MeV/amu U ions on thin and thick solid targets. Initial bare, one-, two-, three-, nine-, and 24-electron ions were used, so that single and multiple ionization of K-, L-, and M-shell electrons and electron capture into bare ions and into ions having initially full or partially full K and L shells could be observed. Multiple-ionization effects in two-electron U ions and in ions having many electrons in the K, L, and M shells are calculated by using the semiclassical approximation and assuming binomial statistics. Binding effects on K-shell ionization are compared with previous measurements using relativistic Xe ions, and with the Glauber theory. For 430- and 955-MeV/amu U ions, good agreement is obtained between measured capture cross sections and calculated radiative and nonradiative (eikonal-approximation) cross sections. Some disagreement is found at lower energies. An approximate model is proposed for multiple-capture cross sections. Finally, the measured equilibrium charge states are compared to ground-state models and to models including excited-state effects. Excited-state effects are less important for relativistic U ions than for any other ion in matter. Differences between the excited- and ground-state models are found to be too small to be observed.

I. INTRODUCTION

Previous papers in this series have considered electron-capture processes (III),[1] K-shell ionization processes (IV),[2] and the equilibrium charge states (II, V) (Refs. 3 and 4) of relativistic heavy ions in matter. Our previous heavy-ion studies have been concerned with 82- to 300-MeV/amu Xe ions. The present paper concentrates on 105- to 955-MeV/amu U ions, extending prior measurements by Gould *et al.*[5]

Whereas previous studies focused mainly on K-shell ionization, we have also made measurements of L- and M-shell ionization using relativistic U ions. Although, at the present high energies, the plane-wave Born approximation (PWBA) (Refs. 6–11) is expected to predict L- and M-shell ionization cross sections accurately, important deviations due to many-electron effects have been discovered by us.[12] The semiclassical approximation[13] and the independent-particle model for multiple ionization[14] were used to predict single and multiple U-ionization cross sections in collisions with targets of arbitrary Z_t.

Section II gives a brief description of the experimental method with particular emphasis on changes made since papers III and IV were published. Section III considers some effects on multiple ionization, omitted from the previous discussion,[12] and examines cases where the agreement between theory and experiment is poor. In Sec. IV, we consider multiple-ionization effects on K-shell ionization in two-electron Xe and U ions, which were previously neglected.[2,5] Comparisons are made with Glauber calculations[15] and between U, Xe, C, and H ions at the same ion velocity relative to the K-shell velocity (v/v_K).

In Sec. V, we consider electron capture by relativistic U and Xe ions. At relativistic velocities, both radiative (REC) and nonradiative (NRC) electron capture are important.[1] For 955-MeV/amu U ions REC is dominant for targets up to $Z_t \approx 50$, while NRC is dominant at 105 MeV/amu above $Z_t \approx 10$. The REC cross sections are calculated using the impulse approximation,[1] which gives the REC cross section in terms of photoionization cross sections.[16] The NRC cross sections are calculated using the eikonal approximation,[17,18] and are compared with the present U-ion data. An approximate model is proposed for multiple-capture cross sections, and is applied to U- and Xe-ion data.

A subtheme in the present series of papers is the investigation of the role of excited states in determining the equilibrium charge states of ions in matter.[3,4] Roughly speaking, for low-Z, many-electron ions in matter, the ions emerge with higher charge states from solid targets

than from gas targets.[19,20] Bohr and Linhard[21] proposed that this is mainly due to electron excitation. Excitation contributes to ionization because excited electrons can be ionized more easily before they decay back to the ground state, producing increased effective ionization cross sections. In papers II and V, models for the equilibrium charge states of low-Z and high-Z (Xe) ions incorporating excited-state effects were found to be in good agreement with experiment. In highly ionized U, few states are long lived because the radiative decay rates scale as high powers of Z. The effect of these states is discussed in Sec. VI and conclusions are drawn in Sec. VII.

II. EXPERIMENT

The measurements were made at the Bevalac accelerator of the Lawrence Berkeley Laboratory. The experimental arrangement was similar to that described in paper III.[1] Incident-ion charge states were prepared by stripping in Mylar, aluminum, or tantalum foils, and were then magnetically selected. They impinged on thin solid targets; the exiting charge states were separated by a dipole magnet, and the dispersed ions were detected by a position-sensitive detector.

In the present measurements, a position-sensitive, delay-line-type parallel-plate avalanche counter was used to detect the charge-state–dispersed ions, similar to the counter described in Ref. 22. The spatial resolution was 4 mm in the vertical and horizontal directions, more than adequate for the 3-cm separation of successive charge states. Although relativistic particles are usually minimally ionizing, the large charge of the U ions provides enough energy loss to initiate the avalanche in the PPAC. The pulse amplitudes obtained with 955-, 430-, and 105-MeV/amu ions ranged from 200 to 300 mV after amplification, comparable to that obtained with ^{252}Cf fission fragments (100 MeV, $Z\sim 50$ ions) with the same amplification. The advantage of using a PPAC is that it is very fast (the pulse lasts less than 50 nsec), allowing data to be accumulated at a high rate. The detector was designed to give both X and Y positions. Although we digitized only the X signal, proportional to the charge state, we displayed the X-Y signal on an oscilloscope to monitor the beam focus.

Ionization and capture cross sections were obtained from the fractions F_i of ions in charge state i, different from the incident charge state. In our previous work,[1] we obtained the cross sections from the intercept at $T=0$ of F_i/T plotted as a function of the solid-target thickness T. Meanwhile, we have found that it is more accurate to integrate the rate equations for the charge fractions in the near-linear region of the F_i dependence on T. Cross sections are then extracted by a least-squares fitting procedure similar to that described in Ref. 20. The solid-target thicknesses were measured by weighing ($T>1$ mg/cm^2), by x-ray attenuation using ^{55}Fe x rays (heavy targets), or by ^{241}Am α-particle energy loss (C targets).

The total error on each extracted cross section has several sources: systematic uncertainty in the background under the relevant charge-state peak in the raw spectrum, statistical error, error in the target-thickness measurement, or uncertainty in the quoted target thickness if the target broke before the thickness could be determined. Furthermore, there is a subtle systematic uncertainty in the least-square fitting procedure of the F_i-vs-T data: the extracted cross section $\sigma(N,n)$ for producing n electrons on the projectile which initially carried N electrons ($N-n=i$) depends on the assumed values of other cross sections $\sigma(N',n')$ which can lead from N to n in two or more steps. As $F_i(T)$ becomes more nonlinear with increasing T, the effect of the cross sections $\sigma(N',n')$ becomes more pronounced. We found empirically that $\sigma(N',n')$ depends mainly on $N'-n'$ and only little on N' (except for $N'\leq 3$). Hence we assumed

$$\sigma(N',N'-i)=(K_N)^{N-N'}\sigma(N,N-i)\ , \tag{1}$$

where i can be positive or negative and K_N is typically close to unity (except for $N\leq 3$).

In the present experiment, careful focusing of the beam reduced any background under the charge-state peak to negligible proportions. In the rare cases in which the background was appreciable, the data were rejected. Total counts in the accumulated spectra were $(1-3)\times 10^4$. The range of values of F_i from $\sim 10^{-3}$ to ~ 0.2 were accepted and 3 to 7 values of T were used in the analysis of a given cross section, giving a typical statistical error of less than 10%.

The remeasurement of quoted target thicknesses indicated typical errors up to 10%, with 5 targets (out of 50) having errors up to 100%. The thin (<0.5 mg/cm^2) Cu, Ag, and Au targets we used were evaporated onto nominally 50-μg/cm^2 C backings. We found typical variations of 20% in the backing thickness. We reanalyzed our earlier Xe-beam data[1,2] with the least-squares fitting procedure, but unfortunately were able to determine only a few target thicknesses by direct measurement.

The systematic uncertainty introduced by the use of Eq. (1) could be assessed in two ways. In some cases, sufficient data were available to include a search for the optimum value of K_N in Eq. (1). In this way, we found that for stripping $K_2\approx 0.5$, $K_3\approx 0.3$, $K_9\approx 0.8$, $K_{24}\approx 1.0$, and for capture $K_N\approx 1.0$ would produce an optimum fit. By arbitrarily varying the values of K_N around these optimal values, we could show that the extracted multiple stripping and capture cross sections of high order could change by as much as a factor of 2, but that the single-charge changing cross sections were hardly affected.

When comparing, in the data presented below, cross sections using the same target set, e.g., U^{83+} and U^{89+} stripping cross sections, we give only the statistical errors. On the other hand, when comparing Xe and U cross sections, we assign a 20% minimum error to the Xe cross sections and a 10% minimum error to the U cross sections to take into account the minimum systematic uncertainties discussed above.

Table I summarizes the incident charge states for which measurements were made. The lack of data at some energies and for some charge states was due to either the unavailability of some incident charge states (e.g., 105-MeV/amu U^{92+}), mistakes (later analysis showed that our intended measurement of 430-MeV/amu U^{89+} was a

TABLE I. Incident charge states.

U charge state	Electronic configuration	Energies (MeV/amu)			
68+	$K^2L^8M^{14}$	955			
83+	K^2L^7	955	430		105
89+	K^2L	955			105
90+	$1s^2$	955	430		105
91+	$1s$			220	105
92+	bare	955	430		

remeasurement of U^{90+}), or running out of accelerator time (this limited the data at 220 MeV/amu).

III. SINGLE AND MULTIPLE IONIZATION

As pointed out in paper IV, the determination of K-shell ionization cross sections from the electron loss of one-electron projectile ions is the cleanest method of studying K-shell ionization cross sections. In contrast to the situation for target K-vacancy production, here capture plays no role as long as sufficiently thin targets are used. As soon as the projectile ion carries more than one electron, multiple-electron loss influences the interpretation of the charge-changing yields, and if more than three electrons are present, electron loss can occur from more than one shell. In line with common usage we call these processes "ionization," but it must be kept in mind that they represent ionization from more than one shell.

The study of these more complex cross sections is of interest since they touch on one of the fundamental problems in atomic physics, the few-electron system. Also, of interest to atomic physics is an, albeit indirect, determination of ionization *probabilities* p_i which enter in a sensitive way into the interpretation of multiple-ionization cross sections since each un-ionized electron contributes a factor $(1-p_i)$ to the total ionization probability of a given shell. For high-Z targets, p_i can be close to unity, and the question of unitarity of the theory must then be faced.[23,24]

Our measurements of multiple-ionization cross sections in 955- and 430-MeV/amu U collisions were presented previously,[12] and were compared with independent-electron approximation calculations.[14] In Sec. III A below, we describe the calculation of some L- and M-shell ionization cross sections that were used in Ref. 12. In Sec. III B, effects on multiple ionization, including the Auger effect, are discussed. Finally, we present data taken with 105-MeV/amu U^{89+} and U^{83+} ions, where the binding effect on L-shell ionization appears to be important. We also reexamine a few of our previous Xe results,[2] where the reevaluation of our data has changed some earlier cross-section values.

A. Independent-electron approximation

The independent-electron approximation assumes that the probability $p_i(b)$ of ionizing an inner-shell electron i at impact parameter b is independent of all other electrons in the atom.[14] This not only allows us to calculate the probability $p_i(b)$ by simply using single-particle (usually hydrogenic) electron wave functions, but also to write the probability of ionizing two electrons i and j as the product p_ip_j. The cross section is obtained by integrating the product of probabilities over impact parameter. In the case where N electrons occupy a shell s, if the probability per electron p_s is assumed to be equal for all N electrons, the binomial theorem gives the probability of ionizing just n electrons without ionizing the remaining $N-n$ electrons:[14]

$$P_s(n,N)=\frac{N!}{n!(N-n)!}p_s^n(1-p_s)^{N-n} . \tag{2a}$$

If one has three shells with N_1, N_2, and N_3 electrons, the cross section for ionizing m electrons is then

$$\sigma_m=\sum_{\substack{n_1,n_2,n_3\\(n_1+n_2+n_3=m)}}\int_0^\infty db\,2\pi bP_1(n_1,N_1)P_2(n_2,N_2)\times P_3(n_3,N_3) . \tag{2b}$$

If more than three shells and more than four electrons are to be ionized, it is easiest to evaluate Eq. (2b) numerically by summing over all possible electron configurations without restricting the sum of the n's to m. For each configuration, $n_1,n_2,n_3,\ldots$, if the sum is equal to say 5, one calculates the integrand $P_1(n_1,N_1)P_2(n_2,N_2)\cdots 2\pi b\,db$ and deposits the value into the $m=5$ bin. If the sum of the n's is 10, the integrand is deposited into the $m=10$ bin, etc. With this method, the amount of computer time needed increases only linearly with the number of initial electrons.

The one-electron ionization probabilities $p_i(b)$ needed in Eq. (2a) were calculated using the semiclassical approximation (SCA) formulation of Hansteen *et al.*[13] Although the PWBA and SCA probabilities are rigorously identical for the ionization of hydrogen atoms, screening in multi-electron atoms or ions affects the Coulomb wave functions of the ionized electron differently in the two approaches, giving different ionization cross sections.[25] These effects are most important for the present high energies (low X values in the tables of Hansteen *et al.*[13]). Hansteen *et al.* give a correction factor μ, which is relevant for the ionization of Ag target atoms, and should be equal to the ratio of the PWBA to SCA ionization cross sections. In the present calculations, we simply normalized the SCA probabilities so that

$$\sigma_s=\int_0^\infty db\,2\pi bp_s(b) \tag{3}$$

is equal to the PWBA cross section per electron for shell s.

To first order, the PWBA cross sections can be calculated using hydrogenic wave functions.[2] For the longitudinal part of the cross section, one need only specify an effective charge Z^* (screened projectile atomic number) and the ionization potential E_i. From these two quantities, the reduced energy $\eta_i=(\beta/Z^*\alpha)^2$ and screening parameter θ_i are calculated, and a reduced cross section can be looked up in tables.[8-11] In the PWBA and SCA, we used Slater screening rules[6] to obtain Z^*, and obtained the ionization potential E_i for highly charged U ions from the tables of Carlson *et al.*[26]

As discussed in IV for K-shell ionization,[2] the PWBA cross sections so obtained neglect four effects: (1) transverse excitation at relativistic velocities,[7] (2) electronic relativistic effects,[27] (3) target-nucleus shielding,[28] and (4) wave-function-distortion effects.[29,30] At relativistic velocities, the additional contribution to the K-shell ionization cross sections due to transverse excitation varies as $(\ln\gamma^2-\beta^2)/\beta^2$.[7] At the highest energy, 955-MeV/amu, this increases the present K-shell ionization cross sections by a factor ~ 1.3. Although transverse ionization cross sections have not been calculated for the L and M shells, we assume that these cross sections will be increased by the same factor as for the K shell.[2,31]

If one uses relativistic electronic wave functions, the U K-shell ionization cross sections are reduced by 10 to 20%.[2] We assume that relativistic electronic effects on the L- and M-shell electrons can be neglected.

For projectile ionization, the perturbing target nuclei are partially screened by the target electrons. Additionally, the target electrons can ionize the projectile electrons in electron-electron collisions, giving rise to the "antiscreening" effect.[28] Uranium L electrons are typically ionized at impact parameters as large as the U L-shell radius. For a target electron to screen the target nucleus in such collisions, its average radial distance from the target nucleus must be much less than the U L-shell radius, which occurs only for the K-shell electrons of targets with $Z_t \gtrsim 50$. Therefore, one can expect very little screening for U K-shell ionization by any target nucleus, slight screening for U L-shell ionization for targets with $Z_t \gtrsim 50$, and screening for U M-shell ionization for $Z_t \gtrsim 30$. One can calculate longitudinal PWBA ionization cross sections with screening,[3] and can define an effective charge ratio Z_t^*/Z_t as the square root of the ratio of PWBA cross sections with and without screening. For 955-MeV/amu U + U collisions, Z_t^*/Z_t is equal to 0.90, 0.95, and 0.99 for the M, L, and K shells, respectively, and is slightly larger at lower energies. Such factors for every Z_t value were incorporated in the present calculations. Antiscreening increases the L- and M-shell ionization cross sections by a factor of $(Z_t^2+Z_t)/Z_t^2$, the linear factor of Z_t coming from Z_t separate electron-electron Coulomb interactions.

The binding or polarization wave-function distortion effects[29,30] were not included in the calculations presented in Ref. 12. They appear to be insignificant for U K-shell ionization at 430- and 955-MeV/amu, as discussed in the following section. In general, they are less important for ionization of L and M electrons, although possible evidence of binding effects on L-shell ionization is seen in our results (Sec. III C below).

The arguments presented in this section actually apply only to the cross-section normalization in Eq. (3). In addition, one must consider whether the nonrelativistic SCA formulation of Hansteen *et al.*[13] is capable of predicting the correct shape of $p_s(b)$ for these high-Z, relativistic collisions. Although the answer to this question is not known presently, for the electronic-relativistic, relativis- tic-velocity, and target-screening effects, we note that the cross-section corrections are small. For the screening effect one could argue that $p_s(b=0)$ is unaffected, but the probabilities at large b are much reduced. Since the cross-section correction, determined by large b values, is at most 10% (for the U M shell), and our experimental uncertainties are of the same magnitude, we do not believe this is a significant correction. Comparisons between nonrelativistic SCA calculations and fully relativistic SCA calculations have not been made for the presently relevant velocities and high-Z ions. For cross sections, the polarization[29,30] and relativistic-velocity effects nearly cancel in the present regime. The corrections for the binding effect on $p_s(b)$ are discussed below.

B. Other sources of multiple ionization

The main contributions to the multiple-ionization cross sections, Eq. (2b), come from the product of independent probabilities. However, antiscreening[28] and Auger transitions may also contribute.

In a collision between a neutral target atom and a uranium ion, one has not just a single Coulomb potential between the perturbing center and the U electron to be ionized, but Z_t+1 separate interactions. One can imagine that if one could line up the target electrons and the target nucleus so they impinge on the U ion with the same impact parameter, one could significantly increase the likelihood of multiple ionization at low Z_t: the target nucleus can ionize the first U electron, a target electron can ionize a second, another target electron can ionize a third, and so on. However, this is unlikely because in reality the target electrons are spread over immense distances compared with the impact parameter relevant to U inner-shell ionization. The likelihood of the target nucleus and electron being sufficiently close together to produce U double-inner-shell ionization is small.

This argument can be made quantitative in the following way. In the presently relevant limit where screening, but not antiscreening, is small, one can write the cross section for single ionization as[28]

$$\sigma_1 = \int_0^\infty db\, 2\pi b[P_1(b)+\rho_e(b)\sigma_e] , \tag{4}$$

where σ_e is the electron-induced projectile ionization cross section and $\rho_e(b)$ is the areal density of target electrons swept through by the projectile:

$$\rho_e(b) = \int_{-\infty}^{\infty} dz\, \rho_t(r) , \tag{5}$$

$$\int_0^\infty \rho_e(b) 2\pi b\, db = Z_t , \tag{6}$$

where $\rho_t(r)$ is the volume density of target electrons. The value $\rho_e(b)$ can be calculated using the Thomas-Fermi model, as described for double REC in III.[1]

Double ionization can come from the double target-nucleus-projectile-electron interaction (term with P_2 below), a target-electron plus nucleus-projectile-electron interaction, or two target-electron-projectile-electron interactions:

$$\sigma_2 = \int_0^\infty db\, 2\pi b[P_2+\rho_e(b)\sigma_e P_1+\rho_e^2(b)\sigma_e^2] . \tag{7}$$

For 955-MeV/amu U^{68+} + C collisions, the calculated

ratio of the double to single ionization cross sections coming from the last two terms of the integrand in Eq. (7) is 2×10^{-4}, which is much smaller than the contribution from the first term or what is found experimentally. Similarly, the target-electron induced effect is negligible in all other cases examined.

The Auger effect is important in U collisions such as U^{68+} where M electrons are present initially. An L-shell electron can be ionized, and one more electron can be lost if the L vacancy decays by Auger-electron emission of an M-shell electron. Since m-fold collisional multiple ionization is approximately proportional to Z_t^{2m} and the ratio of the Auger-induced multiple-ionization cross section to single is independent of Z_t, the influence of the Auger effect is most apparent at low Z_t. In collisions where only K and L electrons are present initially, the Auger effect can contribute only if K holes are created, but since the K-shell ionization is smaller than L-shell ionization, and the Auger yield for U K vacancies is less than 3% in single-vacancy atoms, Auger transitions can be neglected in these systems.

To determine the Auger contribution to two-electron loss in U^{68+}, one must calculate the Auger yield for U^{69+} ions with one L-shell vacancy. Coster-Kronig transitions cannot occur because the usually ejected outer electrons are absent. The $2s$- and $2p$-ionization cross sections are about equal, so we average the Auger yield for the L_1, L_2, and L_3 shells, weighted by the number of electrons. We assume that due to collisional excitation, the 14 M-shell electrons are not in the ground state but are statistically distributed among all the $n=3$ subshells. We can then assume that the LMM Auger transition rate[32] is that for the single-vacancy atom (with 18 M electrons) multiplied by $(13\times14)/(18\times17)$ and that the LM radiative transition rate[33] is reduced by a factor of $\frac{14}{18}$.[34] For the single-vacancy U atoms, the average Auger yield is $\omega_A=0.455$.[32,33] The statistical occupation probabilities reduce it to $\omega_A=0.386$. This factor was used in comparing with the data in Ref. 12. For the convenience of the reader, Fig. 1 reproduces the pertinent figure from Ref. 12. Clearly, at low Z_t, the Auger effect gives the major contribution to double-vacancy formation.

The main Auger contribution to triple ionization in U^{68+} comes from the simultaneous ejection of an L and M electron. In Ref. 12, we neglected the lower occupation of the M shell in calculating ω_A for such a configuration; $\omega_A=0.386$ was used for all other multiple-electron Auger cross sections. The inner-shell ionization cross section used there is the sum of the K- and L-shell cross sections. Most K-shell vacancies decay radiatively to the L shell, contributing directly to the L-vacancy yield; this neglects the small number (less than 20%) decaying radiatively to the M shell. Since N- and outer-shell electrons are absent in U^{68+}, U K vacancies cannot decay to the outer shells.

The U^{68+} measurements at low Z_t provide a way of determining Auger yields for just the M shell. In normal single-vacancy measurements, Auger and radiative transitions are summed over all shells. On the other hand, the charge-state measurements cannot distinguish between $2s$ and $2p$ Auger yields and the M-shell configuration is in an unknown degree of excitation. This may explain the discrepancy between experiment and theory at low Z_t, apparent in Fig. 1.

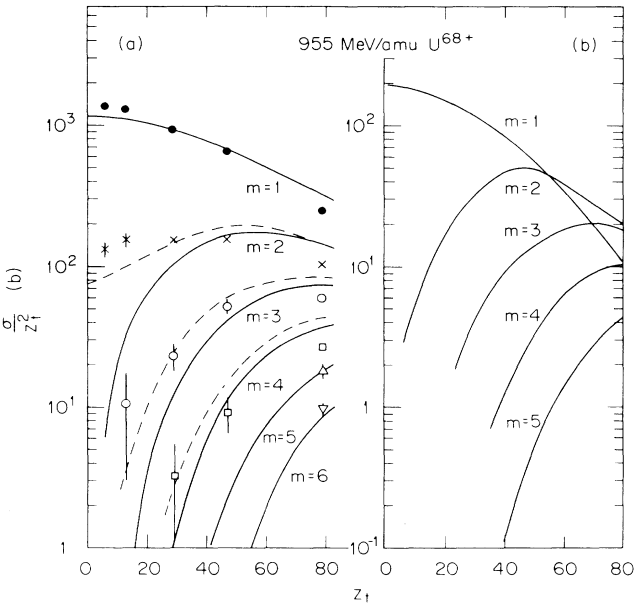

FIG. 1. (a) Measured single- and multiple-ionization cross sections for 955-MeV/amu U^{68+} ions passing through various target foils, as a function of the atomic number Z_t, compared with theory. The cross sections in barns have been divided by Z_t^2. On each curve, m indicates the multiplicity of the stripping process. The solid curves show the independent-electron approximation results. The dashed curves include the computed influence of the LMM Auger effect. (b) Theoretical cross sections for multiple ionization if one vacancy is in the K or L shell.

C. Ionization in 105-MeV/amu U^{83+} and U^{89+} and in Xe^{45+} collisions

The overall agreement between the independent-electron-approximation (IEA) calculations [Eq. (2b)] and experiment[12] seen at 430 and 955 MeV/amu is not found at 105 MeV/amu [Fig. 2(a)]. Wave-function distortion effects, which are more important at lower energies, may account for some of the disagreement, but we do not have a complete explanation for the disagreement. In 105-MeV/amu U^{89+} collisions, U L-shell ionization is dominant. It is possible that the falloff in the reduced single-electron ionization cross sections σ_1/Z_t^2 with increasing Z_t, which is much larger than that predicted by the IEA, is due to the binding effect on L-shell ionization.[29,30] (K-shell ionization contributes less than 5% to U^{89+} single-electron loss. Hence, a possible falloff of the K-shell reduced cross sections with Z_t cannot explain the measured results.)

A difficulty with the binding-energy effect interpretation is that the seven-electron U^{83+} single-ionization cross sections would also be reduced by approximately the same binding factor. But the measured U^{83+} single-ionization cross sections already agree well with the IEA

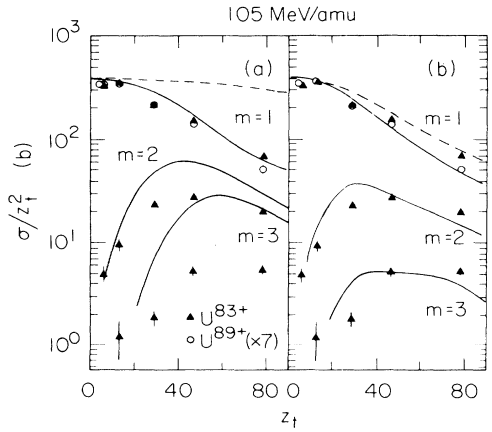

FIG. 2. (a) Measured single-, double-, and triple-ionization cross sections in 105-MeV/amu U^{83+} and single-ionization cross sections in U^{89+} collisions. The cross sections have been divided by Z_t^2. The U^{89+} cross sections are multiplied by 7 to obtain the same magnitude as the seven-electron U^{83+} ones at low Z_t. The dashed curves are calculations for U^{89+} and the solid curves are for U^{83+}. In (b), a binding effect on the theoretical cross sections has been included.

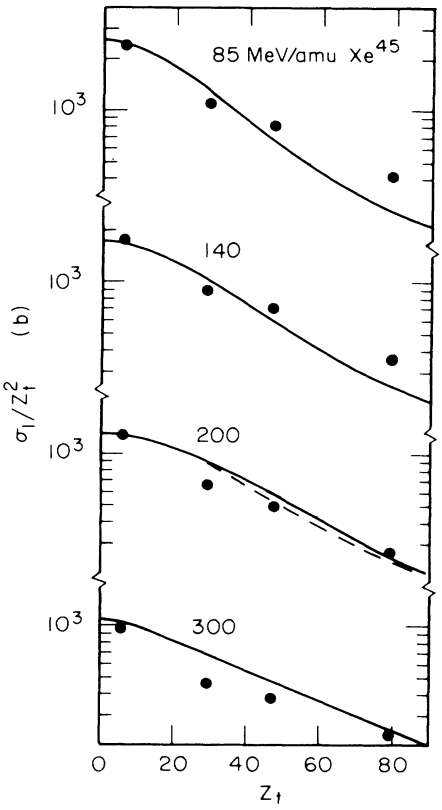

FIG. 3. Measured single-ionization cross sections for 85-, 140-, 200-, and 300-MeV/amu Xe^{45+} ions passing through various target foils as a function of Z_t. The cross sections have been divided by Z_t^2. The solid lines use the unitarization proposal of Ref. 23, where p is replaced by $\sin^2\sqrt{p}$. The dashed line is computed by assuming that $p=0.999$ wherever the SCA value for the ionization probability p exceeds unity.

calculation without introducing a binding effect, although the measured double- and triple-ionization cross sections of U^{83+} disagree strongly with theory. Nevertheless, if we suppose that the ratio of the measured to calculated U^{89+} cross sections is due to a binding-reduction factor that reduces ionization probabilities at all impact parameters uniformly by a factor B, we can calculate the effect on the U^{83+} single- and multiple-ionization cross sections. [This method was also used for double K-shell ionization in IV (Ref. 2) and in Sec. IV below.] Figure 2(b) shows that the introduction of this factor brings the calculated U^{83+} double- and triple-ionization cross sections into slightly better agreement with experiment, although agreement with the single-ionization section becomes worse.

In Fig. 3, we present single-ionization cross sections (divided by Z_t^2) for 85- to 300-MeV/amu Xe^{45+} which also has seven L electrons. Unfortunately, we were unable to measure the target thicknesses of the thinnest targets (Cu, Ag, Au) before these foils broke, so that there is considerable uncertainty connected with the corresponding cross sections. The SCA ionization probabilities at small impact parameters exceed unity at large values of Z_t for these projectiles. (For $Z_t=80$, the $1s$, $2s$, and $2p$ probabilities exceed unity below $b=120$, 250, and 500 fm, respectively.) We used two prescriptions to unitarize the probabilities, one proposed by Wille[23] and used also by Kaneko[24] where p_s is replaced by $\sin^2\sqrt{p_s}$ and the other a simple replacement of the probability p_s in Eq. (1) by 0.999 whenever the SCA value exceeds unity. Both prescriptions give similar results, all of which are in overall qualitative agreement with the data, given the experimental uncertainties.

We conclude that single and multiple ionization in the L and M shells can be approximately understood on the basis of the independent-electron approximation. Nevertheless, for a complete understanding, binding and polarization effects and relativistic-velocity and relativistic-wave-function effects in the SCA must still be computed for the present regime.

IV. K-SHELL IONIZATION

A. Multiple ionization effects

For two-electron ions, the single-electron-loss cross section is given by [cf. Eq. (2b)]

$$\sigma_1(K^2)=2\int_0^\infty db\, 2\pi b p_K(b)[1-p_K(b)]\ , \tag{8}$$

where p_K is the K-shell ionization probability per electron at impact parameter b. This can be compared with the single-electron-loss cross section in one-electron ions,

$$\sigma_1(K^1)=\int_0^\infty db\, 2\pi b p_K(b)\ , \tag{9}$$

from which one obtains

$$\sigma_1(K^1)=\tfrac{1}{2}\sigma_1(K^2)+\sigma_2(K^2)\ , \tag{10}$$

where σ_2 is the double-electron ionization cross section of a two-electron ion. The difference between the one-electron ionization cross sections per K-shell electron for one- and two-electron ions is, therefore, a measure of the double-ionization cross section.

There are two possibilities to test Eq. (10): one experimental, the other theoretical. At 140 and 200 MeV/amu, we were able to extract some double-ionization cross sections from the Xe^{52+} data. Adding these cross sections to one-half of the single-ionization cross sections for Xe^{52+} gives the open-triangle points in Fig. 4. These can be compared directly with the measured Xe^{53+} ionization cross sections shown by open circles. Approximate agreement between the two data sets can be seen, supporting the correctness of Eq. (10).

Before the theoretical cross sections can be compared with the experimental cross sections, the latter have to be corrected for the antiscreening effect of the target electrons.[28] The corrected K-electron cross section is given by[2,35]

$$\sigma_K^{\rm corr}=\sigma_K-Z_t\sigma_e\ , \tag{11}$$

where σ_K is the measured cross section and σ_e is the cross section for K-electron ionization by an electron moving with the projectile velocity v. For σ_e, we used the ionization-cross-section expression of Ref. 36. The correction in Eq. (11) is significant only for $Z_t \lesssim 20$. Figure 4 shows the cross sections $\sigma_1(K^1)/Z_t^2$ and $\sigma_1(K^2)/(2Z_t^2)$ for 82- to 200-MeV/amu Xe^{53+} and Xe^{52+} ions.[2] The differences between the experimental cross sections per electron are of the order of the experimental uncertainties, which are both statistical and systematic because of uncertainties in the target thicknesses. Because of this, in paper IV, the double-loss cross section was neglected; cross sections per electron for single-electron loss in two-electron and one-electron Xe ions were simply averaged.

The fact that the double-electron-loss cross sections are very small in the Xe-ion collisions is consistent with the direct measurements of the double-electron cross sections in 140- and 200-MeV/amu collisions. To fit these cross sections, we assumed that the binding effect reduces uniformly the ionization probability at every impact parameter.[2] The double-ionization cross section is then given by

$$\sigma_2(K^2)=\int_0^\infty db\ 2\pi b[Bp_K(b)]^2\ . \tag{12}$$

The binding reduction factor B can then be taken as the ratio of the measured cross section $\sigma_1(K^1)$ (or theoretical Glauber-approximation cross section) to the PWBA one. The curves in Fig. 4 show the Glauber approximation value for the Xe^{53+} and the Xe^{52+} cross sections calculated using Eqs. (9) and (10). The differences between the two curves are of the order of the experimental uncertainties. This shows that, if the double-ionization cross sections are not measured, it is reasonable to assume that the single-electron ionization cross sections per electron in one- or two-electron ions are approximately equal. For the present U^{90+} ions, where some double-electron ionization cross sections were measured, Eq. (10) was used to obtain $\sigma_1(K^1)$; otherwise we assumed $\sigma_1(K^1)\approx\sigma_1(K^2)/2$.

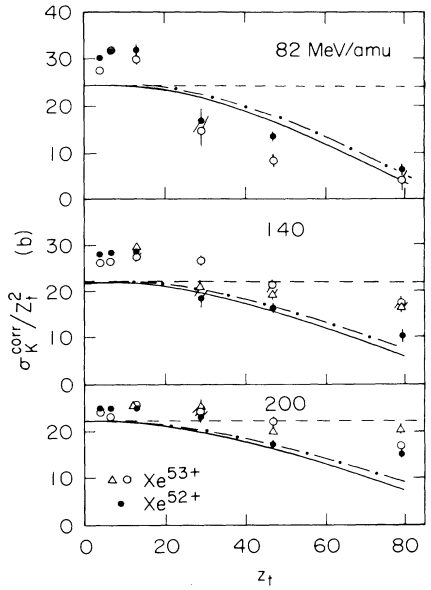

FIG. 4. K-shell ionization cross sections per electron measured using one-electron Xe^{53+} and two-electron Xe^{52+} ions. The cross sections have been corrected for antiscreening according to Eq. (11) and were divided by Z_t^2. The open circles give the measured Xe^{53+} cross sections, and the open triangles give the same cross section computed from the measured single- and double-ionization cross sections of Xe^{52+} according to Eq. (10). The dashed line shows the PWBA prediction, the dashed-dotted curves give the Glauber model for Xe^{53+}, and the solid curves give the Glauber calculations for Xe^{52+}, which include the effect of double ionization.

The marginal fits of the PWBA cross section at low Z_t and of the Glauber theory at high Z_t in Fig. 4 point to possible deficiencies in these theories, not quite so apparent in our earlier work.[2]

B. Comparison of K-shell ionization in U, Xe, C, and H Ions

The scaling laws that are basic to nearly any theory of collision-induced ionization or excitation predict that the cross sections for projectile ionization for any combination of Z_p, Z_t, and v are given by[6]

$$\sigma(Z_p,Z_t,v)=\frac{Z_t^2}{Z_p^4}F\left[\frac{v}{Z_p},\frac{Z_t}{Z_p}\right]\ , \tag{13}$$

where the projectile velocity v is in atomic units. Inner-shell ionization studies are primarily studies of the breakdown of this scaling law. In the PWBA, F does not depend on Z_t/Z_p. However, F is calculated using hydrogenic wave functions so a target-wave-function factor, the screening factor θ_K, is usually present, giving F an additional dependence on Z_t. Binding, polarization,[29,30] and unitarity effects[23,24] give deviations that depend on Z_t/Z_p

and on θ_K. However, for few-electron heavy ions where $\theta_K \approx 1$, as long as one keeps the ratios v/Z_p and Z_t/Z_p constant, identical cross sections should be obtained except for the multiplicative prefactors.

Figure 5 shows measured reduced K-shell ionization cross sections

$$\sigma_{\text{red}} = \frac{\sigma_K^{\text{corr}}}{Z_t^2}\left[\frac{Z_p}{54}\right]^4 \tag{14}$$

for nearly constant v/Z_p plotted against Z_t/Z_p, where σ_K^{corr} is given by Eq. (11). The normalization factors were chosen in Eq. (14) to remove the multiplicative factors in Eq. (13), and to keep the magnitudes of the reduced cross sections the same as in paper IV and in Fig. 4. For the Xe ions, v/Z_p is approximately 1.00 and 1.25 for 82 and 200 MeV/amu, respectively. For the U ions, v/Z_p is approximately 1.08 and 1.29 for 430 and 955 MeV/amu. Also shown in Fig. 5 are data for C^{5+} ions incident on H_2, He, N_2, O_2, and Ne targets (interpolated from measurements[37] at 10, 22, and 42 MeV where v/v_K varies from 1 to 2) and data for p + H collisions[38] (interpolated from measurements between 20 and 40 keV). At low Z_t, the Xe and U data agree well with each other. The C data disagree, possibly indicating that the procedure for subtracting the antiscreening contributions may be incorrect. Antiscreening increases the theoretical $C^{5+} + H^0$ ionization cross section by a factor of 2, but the Xe^{53+}, U^{91+} + Be cross sections by only 1.25, clearly indicating the importance of this correction in the C-ion case. In fact, without subtracting the antiscreening contribution, the experimental C, Xe, and U data are in good agreement. Overall, the Glauber theory is in qualitative agreement with the scaled data, but the generally smaller theoretical values point to an as yet not understood defect in the theory. In particular, it is difficult to understand the apparent lack of scaling between the Xe and U data near $Z_t/Z_p \approx 0.8$.

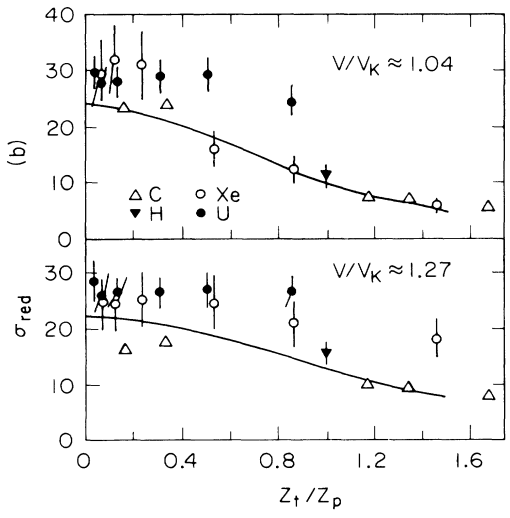

FIG. 5. Reduced, normalized H, C, Xe, and U K-shell ionization cross sections defined by Eq. (14) for approximately equal values of v/v_K plotted against the ratio of perturbing charge to projectile atomic numbers.

Most known effects do not cause a difference between the scaled Xe and U cross sections. Target-electron screening is negligible for these high-Z ions, and antiscreening, which varies relatively as $1/Z_t$, is negligible at the high-Z_t/Z_p values where the differences seem most apparent.[28] Transverse excitation increases the 955-MeV/amu U cross sections by about 30% at all Z_t values due to the relatively large value of v/c. The 200-MeV/amu Xe cross sections are increased only by 5% due to transverse excitation. Electronic relativistic effects are known to increase the U + U K-shell ionization cross sections at ~ 6 MeV/amu by factors of 10^4 over predictions using hydrogenic wave functions.[39] However, as shown in paper IV,[2] these effects give reduced cross sections for all Z_t values at the present large velocities, and practically cancel the increase due to transverse excitation. Hence, these effects cannot explain the possibly larger scaled U cross sections over the Xe ones.

We conclude that presently available ionization theories fail to give more than an approximate account of U K-shell relativistic-projectile ionization by high-Z targets.

V. ELECTRON CAPTURE

At relativistic ion velocities, radiative and nonradiative electron capture are present. At low velocities, the REC cross sections are much smaller than the NRC ones, and have been measured by counting the REC photons.[40] However, at relativistic velocities, REC is the dominant capture process at low Z_t.

Because the REC process is the inverse of the photoelectric process, the REC cross sections can be calculated simply from well-known photoelectric cross sections, as described in III.[1] NRC cross sections are reproduced well by the relativistic eikonal approximation.[17,18] Paper III (Ref. 1) shows that NRC cross sections fit the data only if many excited states of the projectile and the target are included; unlike for low-Z ions and targets,[3] one cannot assume that K- to K-shell capture transitions are dominant.

A. Single-electron capture

Figure 6 compares measured and calculated single-electron-capture cross sections for 430- and 955-MeV/amu U^{90+} and U^{92+} ions. At low Z_t, REC is dominant, and the measured U^{90+} cross sections are much smaller than the U^{92+} ones. For REC, capture into the K shell is dominant, so for U^{90+} ions, where only capture into the L and higher shells is present, much smaller electron-capture cross sections are expected and observed. At high Z_t and at lower projectile velocities, NRC is dominant. The ratio of the U^{92+} to U^{90+} cross sections at high Z_t are smaller than at low Z_t, indicating the higher relative importance of NRC into excited states of the projectile as Z_t increases. The agreement between experiment and the calculated NRC and REC cross sections is good.

The eikonal theory of NRC is a high-energy approximation.[17] It should work best when the ion velocity in atom-

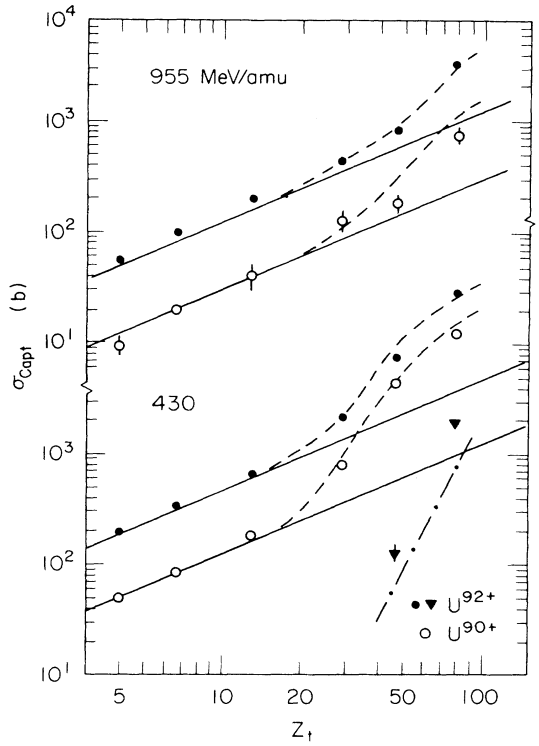

FIG. 6. Measured electron-capture cross sections in 430- and 955-MeV/amu U^{90+} (open circles) and U^{92+} (closed circles) collisions compared with theory. The solid lines show theoretical REC cross sections, the dashed line shows the sum of the calculated REC and eikonal cross sections. The dashed-dotted curve indicates the results of the model discussed in Sec. V B for double-capture cross sections in 430-MeV/amu U^{92+} collisions (triangles).

ic units is much greater than the effective charge of the active electron in either the initial or final state, whichever is greater.[17] According to the scaling theory described in paper III,[1] it is reasonable to take for this criterion the higher value of Z_p/n_p or Z_t^*/n_t, where Z_t^* is a screened target charge and n is the principal quantum number of the state under consideration.[1,17] Although significant differences between measured and calculated NRC cross sections were seen at $Z_t > 50$ in low-Z_p collisions at energies below 200 MeV/amu,[3] smaller deviations were seen in 82- to 200-MeV/amu Xe collisions.[1] Capture into and from the K shell is dominant for low-Z_p ions, so the effective value of n_t there is unity, and, indeed, the discrepancies between theory and experiment are seen where v is less than Z_t^*.[3] However, for Xe and U ions where capture into higher projectile and target shells is present, the breakdown of the eikonal approximation is expected to occur at smaller velocities due to the smaller dominant principal quantum numbers.

B. Infinite-source–infinite-sink model

To investigate the possible breakdown of the eikonal theory at lower velocities, we measured electron capture into U ions in various charge states at 105 and 220 MeV/amu. The interpretation of these measurements is complicated by the presence of multiple-capture processes, not presently computed in the eikonal theory. To compare experiment with theory, small corrections for these multiple-capture processes must be made. To do this, we assume that the theoretical capture probabilities $P_c(b)$ at impact parameter b obey an "infinite-source–infinite-sink" assumption: for any given electron configuration of the target (source) or vacancy configuration of the projectile (sink), so many transitions are possible that reducing the number of electrons in the target or reducing the number of available vacancies in the projectile will have little effect on P_c. This assumption is partly confirmed by the experimental results shown in Fig. 7 which indicate that the single-capture cross section in 105-MeV/amu U^{+q} collisions depend relatively little on q. The assumption works best in situations where capture into excited states is dominant; it cannot be used if $K \rightarrow K$ transitions dominate, i.e., at asymptotically high projectile velocities. On the basis of this model, in multiple capture in a single collision, the capture probability per electron is independent of the other electrons or vacancies and the m-fold capture probability is given by

$$P_m = (P_c)^m \ . \tag{15}$$

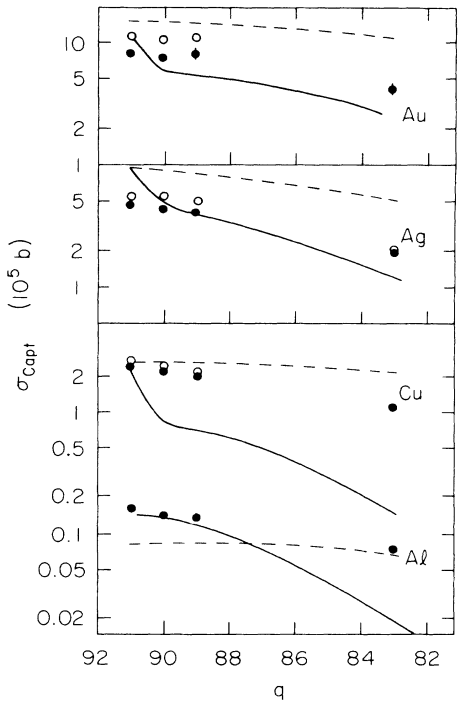

FIG. 7. Capture cross sections in 105-MeV/amu collisions plotted against charge state of the incident U ion. Points with closed circles are experimental single-capture cross sections and those with open circles are single-capture cross sections corrected for multiple-capture effects. The theoretical eikonal approximation cross sections were calculated using a higher-potential (Z/n) criterion for taking either the post or prior form of the eikonal approximation (dashed lines) or using a higher-charge (Z) criterion (solid lines).

All statistical and un-ionized-electron factors, such as those in Eqs. (2) for multiple ionization, are absent in this model. The theoretical m-fold capture cross section is then given by

$$\sigma_m^{\text{th}} = \int_0^\infty db\, 2\pi b (P_c)^m \ . \tag{16}$$

In the present model, this cross section must be interpreted as the cross section for the capture of m electrons, independent of what happens to the other electrons on the target. Hence, σ_m^{th} also contains the possibility of $(m+1, m+2, \ldots)$-fold capture. But, the experimental m-fold capture cross section σ_m^{ex}, as determined by charge state analysis, excludes all higher-order capture. Consequently, experimental and theoretical cross sections in this model are related by

$$\sigma_m^{\text{th}} = \sigma_m^{\text{ex}} + \sigma_{m+1}^{\text{ex}} + \sigma_{m+2}^{\text{ex}} + \cdots \tag{17}$$

or

$$\sigma_m^{\text{ex}} = \sigma_m^{\text{th}} - \sigma_{m+1}^{\text{th}} \ . \tag{18}$$

1. Single-electron capture

Figure 7 shows a comparison between the measured single NRC cross sections for 105-meV/amu uranium 91^+, 90^+, 89^+, and 83^+ and the eikonal approximation.[17,18] (REC has been subtracted from the experimental cross sections, but is not significant compared to NRC at these velocities.) In accordance with Eq. (17), each experimental single-electron capture cross section has been augmented by the sum of the measured multiple-electron capture cross sections. This increases the single-electron capture cross section by at most 30%.

As discussed in paper III,[1] two different criteria can be used in the eikonal calculations for selecting whether the post or prior form of the theory is used.[17] For a given transition between projectile and target shells with principal quantum numbers n_p and n_t, one can take either a "higher charge" or "higher potential" criterion. With the former, one uses the prior form if $Z_p < Z_t$ or the post form (which is always used for U ions) if $Z_t < Z_p$. With the higher potential criterion, one uses the prior form if $Z_p/n_p < Z_t^*/n_t$ and otherwise the post form. (Z_t^* is an appropriately screened nuclear charge for an active electron in the shell n_t.) As Fig. 7 shows, no single criterion works better at every Z_t value, though both come reasonably close to predicting the measured U^{91+}, U^{90+}, U^{89+}, and U^{83+} cross sections. The higher-Z criterion consistently underestimates the cross sections at low charge states, indicating that it does not predict well the relative capture into excited states of the projectile. Also, the smooth charge-state dependence is better predicted by the higher-potential criterion. Nonetheless, factor-of-two differences between the measured and calculated NRC cross sections remain, pointing to the gradual breakdown of the eikonal theory at these lower velocities.[17]

2. Multiple-electron capture

The calculation of multiple-electron capture cross sections from an exact theory is complicated by the many combinations of initial and final states which must be considered in NRC in the present regime.[1] Hence, we propose a somewhat schematic model, based on the infinite-source–infinite-sink assumptions, which reproduces the trends of the multiple-capture cross-section data well. We base this model on the Oppenheimer-Brinkman-Kramers (OBK) development of Lapicki and Losonski[41] who give theoretical expressions for $K \rightarrow K$ and $L \rightarrow L$ capture probabilities and on the relativistic treatment by Moiseiwitsch and Stockmann[42] who treat only the $K \rightarrow K$ case. As is well known, OBK cross sections for single capture differ up to an order of magnitude from experiment.[17] Probably, the OBK capture probability also has an incorrect impact-parameter dependence, although this has not been tested in the present velocity and Z_p, Z_t regime. For these reasons, it is unavoidable that our model should contain an empirical fitting factor.

Following Ref. 41, we write for the theoretical differential single-capture cross section

$$d\sigma_1^{\text{th}} = P_c(b) 2\pi b\, db = \sigma_1^{\text{th}} W(x) x\, dx \ , \tag{19}$$

where

$$x = qb \tag{20}$$

and

$$\int_0^\infty W(x) x\, dx = 1 \ . \tag{21}$$

Hence

$$P_c(b) = \sigma_1^{\text{th}} q^2 W(x)/2\pi \ . \tag{22}$$

The treatment of Ref. 42 and a rederivation by Eichler[43] of the results of Ref. 41 for the relativistic velocity regime show that a relativistically correct expression for q^2 can be written as

$$q^2 = p_-^2 + U_t/I_0 \ , \tag{23}$$

$$p_- = \frac{1}{2I_0}\frac{\alpha}{\beta}\left[\frac{mc^2 - U_p}{\gamma} - (mc^2 - U_t)\right] \ , \tag{24}$$

where U_t and U_p are the electron binding energies in the target and projectile, respectively, $\beta = v/c$ (v = projectile velocity), $\gamma = (1-\beta^2)^{-1/2}$, I_0 is the electron binding energy in H, and α is the fine-structure constant.

From Eq. (16) it now follows that in the present model the theoretical cross section for m-fold capture can be expressed in terms of the single-capture cross section as

$$\sigma_m^{\text{th}} = \sigma_1^{\text{th}} (\sigma_1^{\text{th}} q^2/2\pi)^{m-1} \int_0^\infty W^m x\, dx \ . \tag{25}$$

If we use for $W(x)$ an OBK expression, such as that in Ref. 41 for $K \rightarrow K$ or $L \rightarrow L$ capture [Eq. (A9) or (A10)] or in Ref. 42 for $K \rightarrow K$ capture [Eq. (14)], we can expect the result to differ from a complete theory, because the OBK is not a correct theory, and because many transitions contribute to capture. Also, it is possible that the shape of $P_c(b)$ is not correct in a complete theory. We remedy these potential deficiencies by multiplying the right side of Eq. (25) by a factor f^{m-1} where f is assumed

to be an empirical constant:

$$\sigma_m^{\text{th}} = \sigma_1^{\text{th}} (f \sigma_1^{\text{th}} q^2 / 2\pi)^{m-1} \int_0^\infty W^m x \, dx \ . \tag{26}$$

Comparison is now made with experiment using the relation, based on Eq. (17),

$$\sigma_m^{\text{ex}} = [(\sigma_m^{\text{th}} - \sigma_{m+1}^{\text{th}})/(\sigma_1^{\text{th}} - \sigma_2^{\text{th}})] \sigma_1^{\text{ex}} \ , \tag{27}$$

and substituting for σ_1^{th} the expression given in Eq. (16) with $m = 1$.

In comparing Eq. (27) with our experimental results for 105- and 220-MeV/amu U projectiles and earlier unpublished results[1] for Xe (Figs. 8 and 9), we have found that satisfactory fits can be obtained by assuming that transitions to the projectile L shell dominate in these capture processes as suggested by detailed eikonal calculations. We used experimental $L_{2,3}$ binding energies U_t for the target and calculations of Carlson *et al.*[26] for the L binding energies of partially stripped projectiles. For W we used W_{LL} from Eq. (A11) of Ref. 41 and found that a factor $f \approx 0.15$ gives the best overall fit to the experimental multiple-capture cross sections.

As one can see from Figs. 8 and 9, the proposed model reproduces the trends of the experimental cross sections in a relatively satisfactory manner. In particular, it explains the approximately exponential decrease of the cross sections with increasing multiplicity of the capture, and the steepening of the falloff with decreasing Z_t and with increasing projectile velocity.

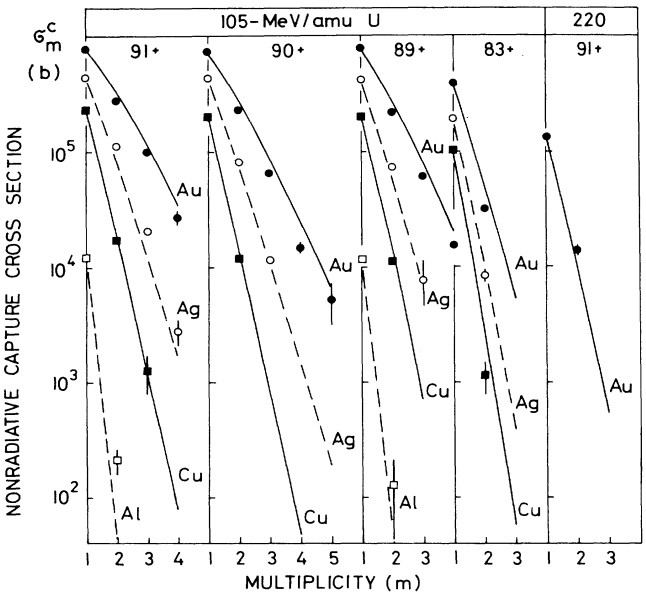

FIG. 8. Multiple-capture cross sections of various charge states of 105- and 220-MeV/amu U ions passing through Al, Cu, Ag, and Au target foils, as a function of the multiplicity (m) of the capture. The theoretical curves are based on the "infinite-source–infinite-sink" model [Eqs. (26) and (27)] and are normalized to the experimental values at $m = 1$.

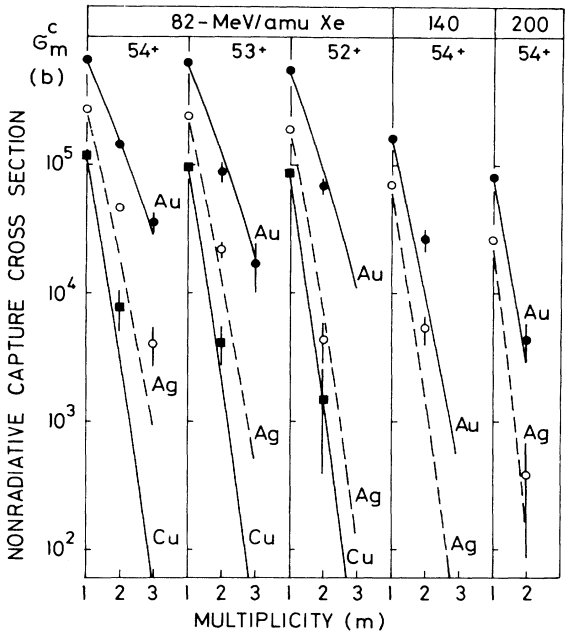

FIG. 9. Same as Fig. 8, but for 82-, 140-, and 200-MeV/amu Xe ions. No Al data are available in this case.

VI. CHARGE-STATE FRACTIONS

A. Equilibrium charge-state-fraction data

Figure 10 shows measured equilibrium charge-state fractions in 430- and 955-MeV/amu U collisions versus target atomic number. The Z_t dependence is typical of

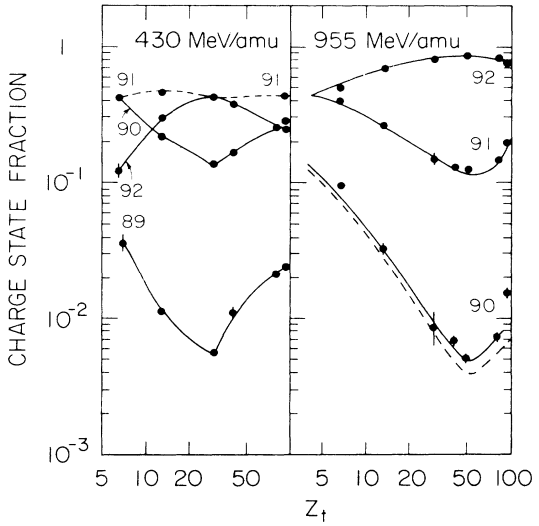

FIG. 10. Measured equilibrium charge-state fractions in 430- and 955-MeV/amu U collisions plotted against target atomic number. For 430 MeV/amu, the lines are to guide the eye. For 955 MeV/amu, the solid and dashed lines have been computed excluding and including excited-state effects, respectively, as described in the text.

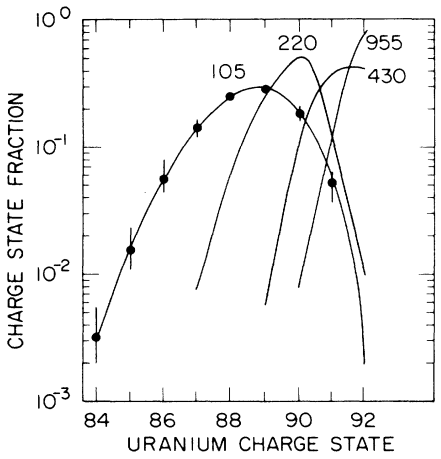

FIG. 11. Measured equilibrium charge-state fractions in 105- to 955-MeV/amu U collisions in Cu or Au (220 MeV/amu only) targets. The lines are to guide the eye.

most other data taken with relativistic ions, and is due to an interplay between the linear Z_t dependence of the REC cross sections, the quadratic Z_t dependence of the ionization cross sections, and the steep ($\sim Z_t^5$) dependence of the NRC cross sections.[3,4] At low Z_t, REC is dominant. Since the REC cross sections increase linearly with Z_t and the ionization cross sections increase quadratically with Z_t, the charge-state fractions for U^{90+}, which are roughly proportional to the square of the ratio of the capture to ionization cross sections, fall off with increasing Z_t. At some intermediate Z_t ($Z_t \sim 30$ for 430 and $Z_t \sim 50$ for 955 MeV/amu), NRC becomes as important as REC. At higher Z_t, the capture cross sections increase faster with Z_t than the ionization ones, so the U^{90+} charge-state fractions increase with Z_t.

Figure 11 shows the measured equilibrium charge-state fractions in Cu (or Au) targets for various ion energies. With decreasing ion velocity, the maximum of the charge-state distribution shifts to lower charge states: Li-like U ions are dominant at 105 MeV/amu, He-like at 220, H-like at 430, and bare ones at 955 MeV/amu. In addition, the charge-state distribution becomes wider at lower velocities.

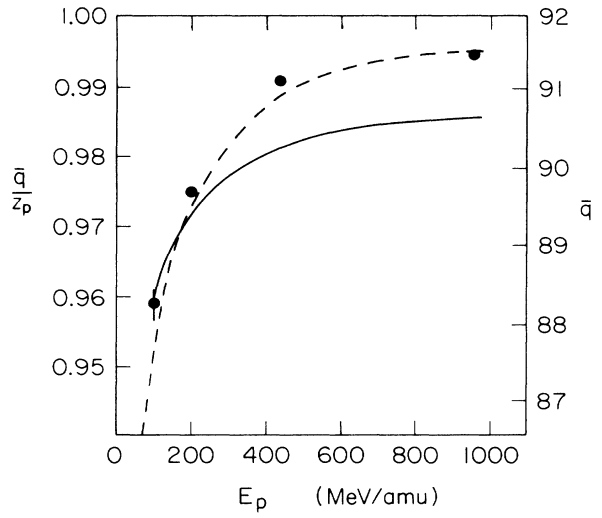

FIG. 12. Average equilibrium charge $\bar{q}/Z_p$ vs energy for U ions. The solid line gives the prediction of the Nikolaev-Dmitriev formula (Ref. 45), and the dashed line, the prediction of Barkas (Ref. 44).

One can calculate an average ion charge using[20]

$$\bar{q} = \sum_i F_i q_i \ , \tag{28}$$

where F_i is the equilibrium fraction of ions having a charge state q_i. Various semiempirical formulas exist in the literature for predicting $\bar{q}/Z_p$ for low-velocity, low-q ions, and are of considerable interest in the design of accelerator strippers and in heavy-ion experiments. The formulas of Barkas[44] and of Nikolaev and Dmitriev[45] are compared with the present data in Fig. 12. The formula of Barkas and the data are in good agreement.

B. Excited-state effects on the charge states of U ions in solid targets

In collisions of low-Z projectiles, higher-charge-state ions emerge from solid targets than from gas targets.[19–21] This is seen in higher values of $\bar{q}$, higher fractions of high-q ions, or lower fractions of low-q ions. The explanation of this effect lies in the effectively lower capture and effectively larger ionization cross sections in solid targets.[21] In low-Z ions, electrons captured into excited states of the projectile are generally ionized before they decay into the ground state, the mean time between ionizing collisions being smaller, in a solid target, than the lifetime of the excited states. Since the excited-state ionization cross sections are generally larger than the ground-state ones, the probability of electron loss is relatively larger, leading to higher charge states. Even if capture into the ground state or decay to the ground state occurs, the effective ionization cross sections could be larger than the ground-state ones, since excitation to the more readily ionized excited states is added to ground-state ionization. In gases, the time between ionizing collisions is sufficiently long, due to the lower target atom density, that decay to the ground state occurs between the collisions.

In paper V,[4] a theory of the charge-state fractions of relativistic 0-, 1-, or 2-electron ions in solid targets, that includes L-shell excited states, is presented. The most sensitive measure of excited-state effects is found in the ratio F_2/F_1 of the equilibrium fraction of two-electron (U^{90+}) to one electron ions (U^{91+}). An analytical formula is derived in V for F_2/F_1:[4]

$$F_2/F_1 = \frac{a_1/2 + a_2 r_2 + a_3 r_3}{(2s_1 + c_1) r_s} \ , \tag{29}$$

where a_1, a_2, and a_3 are capture cross sections into the $1s$, $2s$, and $2p$ states of bare ions, s_1 and c_1 are single- and double-ionization sections, and r_2, r_3, and r_s are measures of the excited-state effects. In gas targets, the excited-state factors r are all equal to unity. In the solid targets, the values of r_2 and r_3 are smaller than unity, since many of

the electrons captured into the excited $2s$ and $2p$ states with cross sections a_2 and a_3 are ionized before they decay to the ground state. The value of r_s multiplying the ground-state ionization cross sections is larger than unity because part of the cross section for excitation to states that are ionized before they decay back to the ground state also contributes to vacancy production.

For U ions, excited-state effects are smaller than for any lower-Z ion, but are still not completely negligible. To compare with ionization cross sections, one can define a decay cross section as

$$\sigma_d = \frac{\lambda}{n_2 v \gamma} , \tag{30}$$

where λ is the decay rate and n_2 is the target-atom density. The decay cross sections for the $2p$, and $1s2p\ ^1P$ and $^3P_1$ states are enormous compared to all ionization and capture cross sections. This is also true in Xe ions. However, in addition, in U ions the $2s$, $1s2s$, $^3S_1$, and $1s2p\ ^3P_2$ states, which are metastable in Xe ions, decay faster than the time between ionizing collisions. Figure 13 shows relative decay cross sections for the $2p$ excited states of H- and He-like U ions.[46–49] The ionization cross sections increase as Z_t^2 and the decay cross sections vary irregularly with Z_t, inversely proportional to the target-atom density [Eq. (30)]. For low Z_t, only the $^3P_0$ and $^1S_0$ states are long-lived enough to affect the r's ($\sigma_d < \sigma_{\text{ioniz}}$). Figure 14 compares the r_2, r_3, and r_s values for Xe and U ions. For $Z_t \sim 10$, r_3 is equal to 0.7 for Xe ions, and 0.95 for U ions. The U r_2 value is also larger than the Xe one, but the r_s values are about the same. The r_s values depend mostly on the $^1S_0$ state which has $\sigma_d < \sigma_{\text{ioniz}}$ for both Xe and U ions.

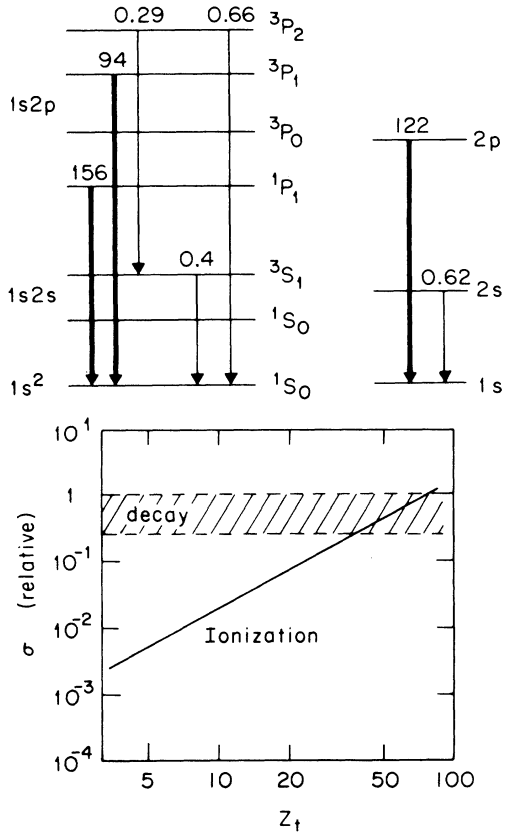

FIG. 13. Relative decay cross sections of $2p$ states in He- and H-like U ions compared with ionization cross sections. The transition rates can be grouped in three sets: those with $\sigma_d(\text{rel}) > 50$, those with $0.1 < \sigma_d(\text{rel}) < 1$, and those with $\sigma_d(\text{rel}) \ll 0.1$, where σ_d is defined in Eq. (30). The first set contains the $2p$, ^1P, and $^3P_1$ states that decay essentially instantaneously compared to collision times, and the last set contains the $^3P_0$ and $^1S_0$ states which are long lived in solid targets. The remaining states decay faster at low Z_t than the time between ionizing collisions but more slowly at high Z_t (the ionization cross sections increase as Z_t^2 but the decay cross sections vary irregularly with Z_t). Although the second group of states is as metastable as the third set for Xe and lighter ions, it decays quickly in U ions due to the strong Z_p dependence of the electric-dipole-forbidden transitions (Refs. 46–49).

Numerical calculations of U-equilibrium-charge-state fractions were made using the same model as described in paper V.[4] The main difference is the incorporation of the decay cross sections of the $2s$, $^3P_2$, $^3P_0$, and $^3S_1$ states[46–49] which were neglected in previous work. The $1s$-ionization and the U^{92+} and U^{90+} capture cross sections were taken from experiment. All other cross sections were either calculated *ab initio* using the PWBA or were calculated relative to the $1s$-ionization cross section and normalized. The right side of Fig. 10 shows the results. (Calculations could be made only for 955-MeV/amu U collisions where three- and more-electron charge fractions are negligible.) The calculated U^{91+} and U^{92+} charge-state fractions cannot be distinguished from experiment. The results for 955-MeV/amu U are similar to those for 200-MeV/amu Xe collisions.[4] The calculated two-electron U^{90+} charge-state fractions including excited-state effects (dashed curve in Fig. 10) are lower than those neglecting excited-state effects (solid lines in Fig. 10, where r_2, r_3, and r_s are all unity). The measurements lie closer to the curve neglecting excited effects, but

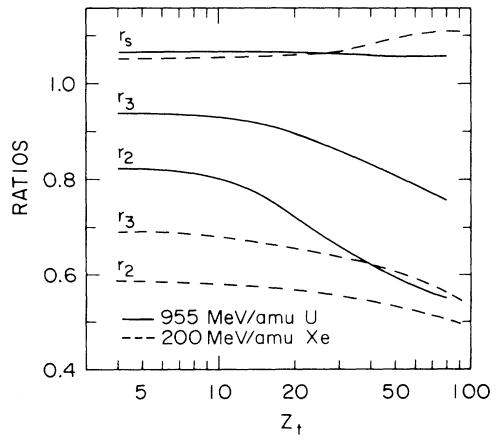

FIG. 14. Theoretical correction factors due to excited-state effects to the ground-state ionization (r_s) and the $2s$ and $2p$ (r_2 and r_3) capture cross sections for 200-MeV/amu Xe ions (dashed lines) and 955-MeV/amu U (solid lines).

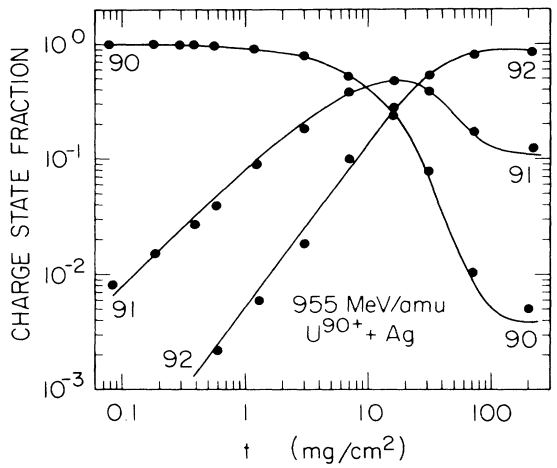

FIG. 15. Calculated and measured target thickness dependence of the charge-state yields in 955-MeV/amu U^{90+} + Ag collisions.

the difference between the dashed and solid curves is too small to be ascertained experimentally. The relative difference between the excited- and ground-state models is larger for Xe ions than for U ions because the values of r_2 and r_3 for U are generally closer to unity. We could not make calculations for 430-MeV/amu U collisions, since three-electron states are then required.

In 955-MeV/amu U^{90+} + Ag collisions, measurements using an especially large range of target thicknesses were made to compare the target-thickness dependence of the charge-state fractions with the results of the numerical excited-state model. As Fig. 15 shows, the calculated charge-state fractions agree with experiment over the whole range thicknesses from low ones (from which the measured ionization and capture cross sections were derived) to equilibrium thicknesses. Here, too, excited-state effects are small, and the data could have been equally well reproduced by the ground-state model.[4]

VII. CONCLUSIONS

This paper represents a culmination of our fundamental studies of inner-shell ionization and capture processes in relativistic heavy-ion atom collisions. The advantage of studying relativistic heavy-ion collisions is that the regime is of sufficiently high energy (i.e., the ion velocity is greater than that of the inner-shell electrons) that one can make use of high-energy approximations as a starting point in formulating cross sections. The PWBA has been used to calculate most ionization and excitation cross sections in this work,[2] and the eikonal approximation has been used for NRC.[1,17] On this basis, we have been able to delineate important effects on inner-shell ionization cross sections such as the screening-antiscreening effect, the binding and polarization effects, and relativistic-velocity and electronic-relativistic effects.[2] We have also been able to develop a model of the charge states of ions in matter that incorporates excited-state effects.[3,4] Although experimental ground-state capture and ionization cross sections are used in this theory, the major progress was made possible by the ability to calculate excitation cross sections and ratios of ionization or capture cross sections *ab initio*.

These theories break down, where expected, at low projectile velocities. For 105-MeV/amu U ions, the L-shell ionization cross sections disagree with the PWBA and the capture cross sections are only qualitatively in agreement with the eikonal approximation. At higher velocities, 10–30% discrepancies remain between the PWBA and measured ionization cross sections at low Z_t, which lie barely outside the range of systematic uncertainties of our data. For K-shell ionization at $v/v_K \approx 1.04$ and 1.27, there is approximate agreement between scaled U, Xe, C, and H cross sections, but some large, unexplained discrepancies are found.

Although it is desirable to extend the excited-state model of the charge states of ions in matter to include more electrons and more states, the numerical complexity makes it unlikely that this will be done. Since excited-state effects are fairly small for the present high-Z, high-charge collisions, gross ion charge states might be predicted *ab initio* using a ground-state model and correction factors (such as r_2, r_3, and r_s in Fig. 14) to account for excited-state effects.

ACKNOWLEDGMENTS

We thank the operators and the staff and management of the Bevalac for making experiments with relativistic few-electron U ions possible. This work was supported in part by National Science Foundation Grant No. PHY-83-13676 (at Stanford University), by the Director, Office of Energy Research, Office of Basic-Energy Sciences, Chemical-Science Division of the U.S. Department of Energy under Contract No. DE-AC03-76SF00098 (at Lawrence Berkeley Laboratory), and by the U.S. Department of Energy under Contract No. DE-AC02-76CH00016 (at Brookhaven National Laboratory).

*Permanent address: Department of Physics, Tsinghua University, Beijing, People's Republic of China.

[1]W. E. Meyerhof, R. Anholt, J. Eichler, H. Gould, Ch. Munger, J. Alonso, P. Thieberger, and H. E. Wegner, Phys. Rev. A **32**, 3291 (1985) (paper III).

[2]R. Anholt, W. E. Meyerhof, H. Gould, Ch. Munger, J. Alonso, P. Thieberger, and H. E. Wegner, Phys. Rev. A **32**, 3302 (1985) (paper IV).

[3]R. Anholt, Phys. Rev. A **31**, 3575 (1985) (paper II).

[4]R. Anholt and W. E. Meyerhof, Phys. Rev. A **33**, 1556 (1986) (paper V).

[5]H. Gould, D. Greiner, P. Lindstrom, T. J. M. Symons, and H.

Crawford, Phys. Rev. Lett. **52**, 180 (1984).
[6]E. Merzbacher and H. W. Lewis, in Vol. 34 of *Encyclopedia of Physics,* edited by S. Flügge (Springer, Berlin, 1958), p. 166.
[7]R. Anholt, Phys. Rev. A **19**, 1004 (1979).
[8]G. S. Khandelwal, B. H. Choi, and E. Merzbacher, At. Data **1**, 103 (1969).
[9]B. H. Choi, E. Merzbacher, and G. S. Khandelwal, At. Data **5**, 291 (1973).
[10]R. Rice, G. Basbas, and F. McDaniel, At. Data Nucl. Data Tables **20**, 503 (1970).
[11]D. E. Johnson, G. Basbas, and F. D. McDaniel, At. Data Nucl. Data Tables **24**, 1 (1979).
[12]W. E. Meyerhof, R. Anholt, X.-Y. Xu, H. Gould, B. Feinberg, R. J. McDonald, H. E. Wegner, and P. Thieberger, Phys. Rev. A **35**, 1967 (1987).
[13]J. M. Hansteen, O. M. Johnsen, and L. Kocbach, At. Data Nucl. Data Tables **15**, 305 (1975).
[14]J. H. McGuire and O. Weaver, Phys. Rev. A **16**, 41 (1977).
[15]J. H. McGuire, Phys. Rev. A **26**, 143 (1982).
[16]J. H. Scofield, University of California Report No. UCRL-51326 (unpublished).
[17]J. Eichler, Phys. Rev. A **32**, 112 (1985).
[18]R. Anholt and J. Eichler, Phys. Rev. A **31**, 3505 (1985).
[19]H. D. Betz and L. Grodzins, Phys. Rev. Lett. **25**, 903 (1970).
[20]H. D. Betz, Rev. Mod. Phys. **44**, 465 (1972).
[21]N. Bohr and J. Lindhard, K. Dan. Videns. Selsk. Mat.-Fys. Medd. **28**, 1 (1954).
[22]Y. Eyal and H. Stelzer, Nucl. Instrum. Methods **155**, 157 (1978).
[23]U. Wille, J. Phys. B **16**, L275 (1983).
[24]T. Kaneko, Phys. Rev. A **32**, 2175 (1985).
[25]O. Aashamar and L. Kocbach, J. Phys. B **10**, 869 (1977).
[26]T. A. Carlson, C. W. Nestor, N. Wasserman, and J. D. McDowell, At. Data **2**, 63 (1970).
[27]P. A. Amundsen, L. Kocbach, and J. M. Hansteen, J. Phys. B **9**, L203 (1976).
[28]J. H. McGuire, N. Stolterfoht, and P. R. Simony, Phys. Rev. A **24**, 97 (1981).
[29]G. Basbas, W. Brandt, and R. Laubert, Phys. Rev. A **17**, 1655 (1978).
[30]G. Basbas, W. Brandt, and R. Laubert, Phys. Rev. A **7**, 973 (1973).
[31]R. Anholt and H. Gould, Adv. At. Mol. Phys. **22**, 315 (1986).
[32]E. J. McGuire, Phys. Rev. A **3**, 587 (1971).
[33]J. M. Scofield, Phys. Rev. **179**, 9 (1969).
[34]F. P. Larkins, J. Phys. B **4**, L29 (1971).
[35]R. Anholt, Phys. Lett. **114A**, 126 (1986).
[36]M. R. H. Rudge and S. B. Schwartz, Proc. Phys. Soc. London **88**, 563 (1966).
[37]R. Anholt, X.-Y. Xu, W. E. Meyerhof, Ch. Stoller, J. D. Molitoris, B. Rude, and R. J. McDonald (unpublished results).
[38]J. T. Park, Ad. At. Mol. Phys. **19**, 67 (1982). See also Fig. 4 of Ref. 2.
[39]R. Anholt, H. H. Behncke, S. Hagmann, P. Armbruster, F. Folkmann, and P. H. Mokler, Z. Phys. A **289**, 349 (1979).
[40]P. Kienle, M. Kleber, B. Povh, R. M. Diamond, F. S. Stephens, E. Grosse, M. Maier, and D. Proetel, Phys. Rev. Lett. **31**, 1099 (1973).
[41]G. Lapicki and W. Losonski, Phys. Rev. A **15**, 896 (1977).
[42]B. L. Moiseiwitsch and S. G. Stockmann, J. Phys. B **13**, 2975 (1980).
[43]J. Eichler (private communication).
[44]W. H. Barkas, *Nuclear Research Emulsions* (Academic, New York, 1963), Vol. I, p. 371.
[45]V. S. Nikolaev and I. S. Dmitriev, Phys. Lett. **28A**, 277 (1968).
[46]C. D. Lin, W. R. Johnson, and A. Dalgarno, Phys. Rev. A **15**, 154 (1977).
[47]M. Hillery and P. J. Mohr, Phys. Rev. A **21**, 24 (1980).
[48]G. W. F. Drake, Nucl. Instrum. Methods Phys. Res. B **9**, 465 (1985).
[49]C. Munger and H. Gould, Phys. Rev. Lett. **57**, 2927 (1986).